Article

Highly uniform gold nanobipyramids for ultrasensitive colorimetric detection of influenza virus

Shaohua Xu, Wenjun Ouyang, Peisi Xie, Yi Lin, Bin Qiu, Zhenyu Lin, Guonan Chen, and Longhua Guo

Anal. Chem., **Just Accepted Manuscript** • DOI: 10.1021/acs.analchem.6b03711 • Publication Date (Web): 26 Dec 2016

Highly uniform gold nanobipyramids for ultrasensitive colorimetric detection of influenza virus

Shaohua Xu, Wenjun Ouyang, Peisi Xie, Yi Lin, Bin Qiu, Zhenyu Lin*, Guonan Chen and Longhua Guo*

Institute of Nanomedicine and Nanobiosensing, Ministry of Education Key Laboratory of Analysis and Detection for Food Safety, Fujian Provincial Key Laboratory of Analysis and Detection Technology for Food Safety, College of Chemistry, Fuzhou University, Fuzhou, 350116, China.

*E-mail: guolh@fzu.edu.cn; zylin@fzu.edu.cn

ABSTRACT: Gold nanoparticles (AuNPs) have been frequently utilized for the construction of diverse colorimetric biosensors. Normally, AuNPs with sharp edges could have better sensitivity. However, the poor monodipersity of AuNPs with sharp edges seriously confines their utility for colorimetric biosensing. Herein, we demonstrate the utility of highly uniform gold nanobipyramids (Au NBPs) for ultra-sensitive colorimetric detection of H_5N_1 virus. The proposed method is based on the fact that alkaline phosphatase (ALP) could catalyze the decomposition of 4-Aminophenyl phosphate (4-APP) to generate 4-aminophenol (4-AP), which would then reduce silver nitrate to metal silver, and then deposited on Au NBPs. The metal silver shell coated on the Au NBPs changed the refractive index of gold and thus resulted in a blue shift of longitudinal localized surface plasmon resonance (LSPR) and accompanied a vivid color change. This method exhibited a higher sensitivity than that of other Au NPs such as gold nanorods due to the high-index-faceted on the tips of the Au NBPs. This method was used to detect the activity of ALP. It exhibited a linear range of 0.1 ~ 5 mU/mL with a limit of detection (LOD) of 0.086 mU/mL. Finally, the proposed method was used in immunoassay to detect H_5N_1 virus. The results showed that the corresponding linear range for the detection of H_5N_1 virus antigen was 0.001 ~ 2.5 ng/mL, and the LOD was determined to be 1 pg/mL, which is more sensitive than those in most of the colorimetric biosensors reported previously.

Keywords: colorimetric biosensor; gold nanobipyromid; localized surface plasmon resonance; influenza virus.

1. Introduction

Rapid identification and quantification of contagious virus is great significant in prompt treatment and effective management for illness. Detection of pathogen with high sensitivity and selectivity was regarded as the key for preventing problems from further spreading[1,2]. However, current approaches for ultrasensitive detection of biomarkers often need sophisticated instruments and professional operating, such as those approaches based on fluorescence[3], electrochemistry[4,5], electrochemiluminescence[6], and surface enhanced raman scattering (SERS)[7]. In contrast, colorimetric assay shows obvious superiority for its simplicity, convenience, low cost and the possibility to be readout by naked eyes[8,9,10]. Nevertheless, the relatively low sensitivity of conventional colorimetric biosensors limits the widespread application. Hence, it is significant to exploit a sensitive and selective colorimetric approach.

Noble metal nanomaterials have attracted great interest owing to their excellent physical and chemical properties[11,12,13]. Of all kinds of noble metal nanomaterials, gold nanorods (Au NRs) show great potential for the fabrication of different kinds of biosensors and chemical sensors due to their highly controllable shape and tunable localized surface plasmon resonance (LSPR) peak from visible to near-infrared range[14,15,16,17]. However, disadvantages still exist. Firstly, the relatively wide size and shape distributions of Au NRs may make the longitudinal plasmon peaks inhomogeneously broadened[18,19,20]; secondly, the round end shape of Au NRs offers a relatively small local electric field enhancement which limits the application of plasmon enhanced spectroscopy[20]. As an alternative, Au nanobipyramids (Au NBPs) have received much attention because of their intriguing optical properties. For example, both the extinction cross-sections and local electric-field enhancements of Au NBPs are much larger than those of Au NRs[21,22]. As a result, Au NBPs exhibit a higher sensitivity to refractive index and a larger figure of merit[23,24]. Moreover, the LSPR properties of Au NBPs can also be turned from visible to near-infrared region[25], enabling them a promising nanomaterial for

different applications. For example, Zhang et al.[26] demonstrated Au NBPs can be used as saturable absorbers for ultrafast pulsed-laser application; Liu et al.[27] used Au NBPs to enhance the circular dichroism (CD) signal for DNA detection. The results showed that the plasmonic CD exhibits good sensitivity and reproducibility. Although these methods have shown advanced applications, the shortcomings are also obvious, such as a broaden LSPR peak or insensitivity to the targets. The main reason is that the Au NBPs used for those applications are not uniform. It is only until recently that the synthesis of highly homogenous Au NBPs have been reported[28].

Enzyme-linked immunosorbent assay (ELISA) is known for its high selectivity due to the specific recognition between antibody and antibody and has been widely employed in clinical diagnosis[29,30], environmental monitoring[31,32], food safety[33,34] and so on. Most of the commercial ELISAs currently use horseradish peroxidase (HRP) as the enzyme label and 3,3',5,5'-tetramethylbenzidine (TMB) as the chromogenic substrate. The targets are usually quantified by the optical density of a yellow compound (TMB_{oxi}). Human eyes are insensitive to optical density changes of the same color, so it is not suitable for sensitive detection of targets by the naked eyes. To improve the visual detection sensitivity, it is key to develop an immunoassay approach that shows multicolor changes. To meet this challenge, many investigations have been done. For example, Roberto de la Rica et al.[35] employed hydrogen peroxide as the reductant for the growth of gold nanoparticles, and an ultra-low detection limit of 10^{-18} g/mL was achieved for the detection of a target protein; Zhang et al[36] designed a gold nanoparticle-aggregation based sensor for the detection of H_7N_9 virus. The detection limit was as low as 25 pg/mL. All the above-mentioned approaches have exhibited good sensitivity. Regretfully, the accuracy for the determination of targets with the naked eyes could still be a big challenge.

In this work, we developed a colorimetric immunoassay method for the ultrasensitive detection of H_5N_1 virus. This method was based on the growth of silver shell on the Au NBPs in the presence of silver ion and 4-aminophenol (4-AP); 4-AP was produced via the catalysis of 4-aminophenyl phosphate monosodium salts (4-APP) by alkaline phosphatase (ALP). Owning to the sharp tips of the Au NBPs, significant response was observed in a target concentration as low as 1.0 pg/mL. More interestingly, a multiple of naked-eye distinguishable colors were observed in response with different concentrations of H_5N_1 virus antigen. As a consequence, our proposed approach may be used for the semi-quantitative determination of the H_5N_1 virus in biological samples with the naked eye.

2. Experimental section

2.1 Materials and regents

Chloroauric acid tetrahydrate ($HAuCl_4{\bullet}4H_2O$), cetyltrimethylammonium bromide (CTAB), ammonium hydroxide ($NH_3{\bullet}H_2O$, 25%), sodium citrate, silver nitrate ($AgNO_3$), and hydrogen peroxide (H_2O_2, 30%) were purchased from Sinopharm Chemical Reagent Co. Ltd. (Shanghai, China). Ascorbic acid (Vc) and diethanolamine (DEA) were obtained from Aladdin (Shanghai, China). Bovine serum albumin (BSA) and Tween 20 were purchased from Glenview (USA). Sodium borohydride ($NaBH_4$) was purchased from Sigma-Aldrich (USA). Cetanecyltrimethyl ammonium chloride (CTAC) was obtained from BBI Life Sciences (Shanghai, China). Sodium orthovanadate (Na_3VO_4) was obtained from Macklin (Shanghai, China). ALP (25.8 U/mL) was obtained from Worthington (USA). 4-APP (Santa Cruz Biotechnology, Inc. USA) was used throughout the work. Mouse anti-H_5N_1 hemagglutinin monoclonal antibody (Ab_1), biotinylated rabbit anti-H_5N_1 hemagglutinin polyclonal antibody (Ab_2) and H_5N_1 hemagglutinin standard were purchased from Sino Biological Inc. (Beijing, China). Streptavidin alkaline phosphatase was purchased from Promega (USA). All high-binding polystyrene 96-well single-break strip plates were purchased from Thermo Fisher Scientific (USA). All other reagents were of analytical grade without further purification, and millipore purification system-based ultrapure water was used throughout this study (18.2 MΩ·cm, Milli-Q, Millipore). All photographs were recorded by a Canon EOS 600D digital camera (Japan). The human serum specimens were obtained from the Hospital of Fuzhou University (Fujian, China).

2.2 Synthesis and purification of Au NBPs.

Au NBPs were synthesized according to the typical seed-mediated method[25]. The freshly prepared ice-cold $NaBH_4$ (0.01 M, 0.6 mL) was added to the mixed solution containing $HAuCl_4$ (0.01 M, 0.5 mL), trisodium citrate (0.01 M, 1 mL), and water (38.5 mL) under vigorous stirring. Then the orange red seed was aged at least 5 h in dark before use. A volume of gold seed solution (5.0 mL) was injected to the growth solution, which was prepared in advance by mixing CTAB (0.1 M, 200 mL), $HAuCl_4$ (0.01 M, 10 mL), $AgNO_3$ (0.01 M, 2 mL), hydrochloric acid (HCl, 1 M, 4 mL), and Vc (0.1 M, 1.6 mL), followed by gentle shaking for about 2 min. The color of the mixed solution turned to purple red after the addition of seed. Then the mixture was left for undisturbed at water bath overnight (30 ℃). The longitudinal plasmon wavelength of the as-prepared Au NBPs was around 750 nm.

The purification of Au NBPs was followed by a three-step method[20]. Firstly, the resulting Au NBPs sample (200 mL) was centrifuged at 10000 rpm for 15 min. The precipitate was redispersed in CTAC (0.08 M, 150 mL), followed by the addition of $AgNO_3$ (0.01M, 40 mL) and Vc (0.1 M, 20 mL); then the resultant solution was kept in an oil bath (65 ℃, 4 h) to produce Au@Ag core-shell nanorods. The as-prepared Au@Ag core-shell nanorods was centrifuged at 6000 rpm for 15 min, and the precipitate was redispersed by CTAB (0.05 M, 150 mL). The solution was kept undisturbing for at least 4 h. The rod-like Au@Ag nanomaterial precipitated, while other shaped nanoparticles stayed in the supernatant. Then the supernatant was discarded, and the precipitate was redispersed in water (100 mL). The redispersed Au@Ag core-shell nanorods solution was gently mixed with $NH_3{\bullet}H_2O$ (25%, 10 mL) and H_2O_2 (5%, 1 mL) and kept undisturbing for 4 h. The Ag segments wrapped on the Au NBPs were etched and AgCl precipitate was formed during the process. Finally, the supernatant was taken out carefully and centrifuged at 8000 rpm for 15 min. After that, the product was redispersed with a CTAB solution (0.05 M, 100 mL) for further use.

2.3 Colorimetric determination of ALP

ALP was carefully diluted by DEA buffer (pH 7.6) to different concentration (0.1 ~ 50 mU/mL). Au NBPs (50 μL, 1.0 a.u. at 750 nm), 4-APP (50 μL, 2.0 mM in 0.4 M pH 9.8 DEA

buffer), and $AgNO_3$ (50 μL, 10 mM) were added to a 96-well plate (as the substrate solution). ALP standards with various concentrations in DEA buffer (10 μL) were added simultaneously to the substrate solution and incubated for 35 min at 37 ℃. Na_3VO_4 (50 μL, 10 mM) was added to the resulting solution to inhibit the activity of ALP. Such solution was then monitored by a Microplate Spectrophotometer (Multiskan GO, Thermo Scientific, USA) or distinguished with the naked eyes.

2.4 Detection of H_5N_1 virus

Before detection, a functionalized procedure was performed to immobilize the capture antibody on a 96-well plate. Briefly, capture antibody (100 μL, 0.5 μg/mL) in carbonate buffer (pH 9.6) was added to the 96-well plate and incubated over night at 4 ℃. Then the plate was washed by 0.05 % tween 20-Tris-HCl buffer (TBST buffer) three times. After that, bovine serum albumin (300 μL, 3%, BSA) was injected into each well and incubated 1 h at 37 ℃ to block the plate. During these processes, the capture antibody was immobilized on the plate. Different concentrations of H_5N_1 virus standards or serum samples (100 μL) were added to each plate and incubated at least 60 min at 37 ℃. After washing the plate, biotinylated detection antibody (100 μL, 0.5 μg/mL) was added to each well and incubated for another 60 min at 37 ℃, followed by the addition of avidin-ALP (100 μL) and incubation for 30 min at 37 ℃. Au NBPs (50 μL, 1.0 a.u. at 750 nm), 4-APP (50 μL, 2.0 mM in 0.4 M pH 9.8 DEA buffer), and $AgNO_3$ (50 μL, 10 mM) were added to the wells and incubated for 35 min at 37 ℃. Finally, Na_3VO_4 (50 μL, 10 mM) was added to each well to stop the reaction and then the UV-vis spectra were measured by a microplate spectrophotometer in a range of 300 − 1000 nm.

3. Results and Discussion

3.1 Characterization of Au NBPs and principle of the proposed biosensor

In this work, the colorimetric signals mainly result from enzyme-induced silver deposition on the surface of the Au NBPs. Therefore, one key factor of this assay is the synthesis of Au NBPs with high monodispersity. However, the purity of as-grown Au NBPs usually is no more than 60% by the seed-mediated growth method[28], which limits the application of this promising nanomaterial for biosensing. After three-step purification, Au NBPs with high monodispersity were obtained in this study. As shown in Figure S1A, the as-grown Au NBPs exhibited two approximate intensity LSPR peaks at ~550 nm and ~750 nm, respectively, indicating that many spherical particles and impurities coexist. After the three-step purification, the intensity at ~550 nm significantly decreased and the LSPR peak slightly blue shifted, demonstrating that the sphere nanoparticles and impurities are removed. The transmission electron microscope (TEM) image shown in Figure S1B further verifies the high monodispersity of Au NBPs after purification.

As shown in Scheme 1, when target antigen (e.g. H_5N_1) existed, the capture antibody (Ab_1), antigen, and detection antibody (Ab_2) formed a sandwiched immunocomplex (Ab_1-antigen-Ab_2) via antibody-antigen interaction. Then the sandwiched immunocomplex was conjugated with ALP through biotin-avidin interaction. 4-APP was hydrolyzed in the presence of ALP, and the produced 4-AP could reduce silver nitrate to silver monomer. The silver monomer was then deposited on the surface of Au NBPs, which results in a LSPR peak blue-shifted and meanwhile the color of the solution changed from brownish red to green and even red in response with different thickness of silver deposition. No immunocomplex formed without target antigen. Thus, both the LSPR and solution color were unaltered. Owing to the vivid color response, the target concentration could be easily distinguished with the naked eyes or detected with a spectrometer by the LSPR peak shifts.

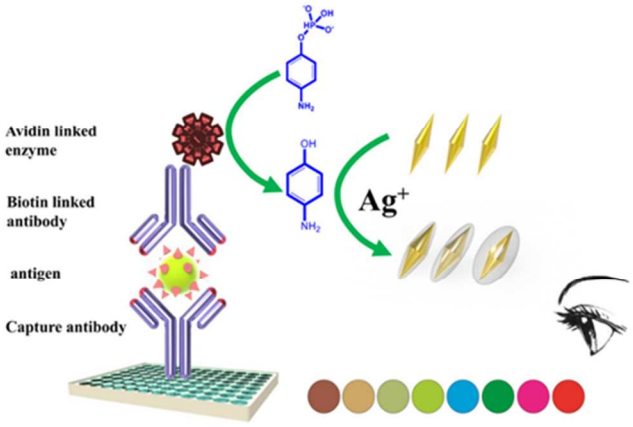

Scheme 1 Schematic illustration of the principle of the proposed immunosensor

To verify the reduction of silver nitrate by 4-AP, a transmission electron microscope (TEM) study was carried out. As shown in Figure 1A, B, and C, the original Au NBPs were standard bipyramid shape with a brownish red color (Figure 1A). After the deposition of Ag, the bipyramid nanostructures were cylinder like shape and the solution color was green (Figure 1B). When almost all silver precursors were reduced, the nanostructures were “walnut-like”. The solution color was red (Figure 1C). Simultaneously, the LSPR peak blue-shifted from 750 nm to 580 nm (Figure 1D). It is worth to note that this silver deposition process is significantly different from that of Au NRs, which is one side deposition on the surface[37,38]. In this work, Ag is deposited uniformly around the Au NBPs side and formed a “walnut-like” nanostructure. This is because the side surface of Au NBPs is high-index-faceted, and the deposition of Ag on the side facet may lower the surface energy[39]. The surfactant used in this work is Tween 20 rather than CTAC or CTAB, which may be another reason for the formation of “walnut-like” Au NBPs@Ag. The CTAB molecule could selectively bind to [110] facets strongly and thus minimizes the overall surface energy[40]. As a result, a different growth rate is presented between [110] and [100] facets of gold nanorods, and then an anisotropic coating is formed. While in this case, none CTAB was existed around the Au NBPs, thus the silver coating process was homogeneous.

To further verify the production of 4-AP by ALP hydrolysing 4-APP, a control study was performed. As shown in Figure 1E, when only 4-APP was mixed with silver nitrate and Au NBPs, the color remained unchanged, and no LPSR peak shift was observed. After the addition of ALP, the color turned to

green immediately, and the LSPR peak blue-shifted significantly. In addition, both the solution color and the LSPR peak were similarly when ALP and 4-APP were replaced by 4-AP. These results demonstrate that only 4-AP can lead to the silver deposition, while 4-APP cannot reduce silver nitrate to silver element.

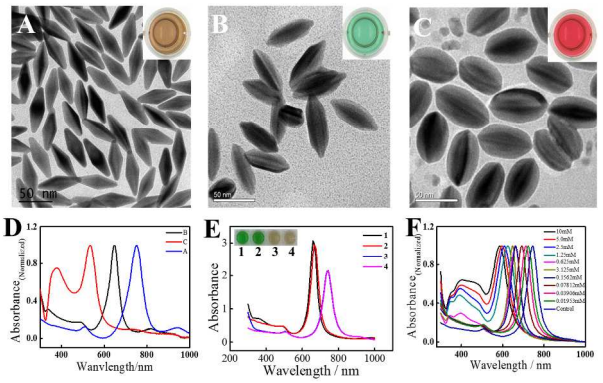

Figure 1 (A) UV-vis absorption spectra of (1) 50 μL 1 mM 4-AP + 50 μL 10 mM Ag^+ + 50 μL Au NBPs, (2) 10 μL10 mU/mL ALP + 50 μL 2 mM 4-APP + 50 μL 10 mM Ag^+ + 50 μL Au NBPs, (3) 50 μL 10 mM 4-APP + 50 μL 10 mM Ag^+ + 50 μL Au NBPs, (4) 50 μL Au NBPs. (B) TEM and photographs of the Au NBPs in the absence (B) and in the presence of different thickness of silver deposition (C, D) and their corresponding UV-vis absorption spectra (E). (F) UV-vis absorption spectra of silver nitrate reduced by different concentration of 4-AP and deposited on Au NBPs.

The UV-vis extinction spectra of the nanostructures deposited with different thickness silver are shown in Figure 1 F. The longitudinal and transverse LSPR peaks of the starting Au NBPs were located at ~750 nm and ~520 nm, respectively. After the deposition of Ag, both the longitudinal and the transverse LSPR peaks blue shifted, owing to the surrounding refractive index change of Au NBPs. And two new peaks at around 350 nm and 400 nm emerged; this may be attributed to the transverse multipolar plasmon mode of the Au NBP@Ag nanostructures and the plasmon resonance of bulk Ag, respectively.[39]

In a word, the principle of this work could be divided into two parts: firstly, the formation of sandwiched immunocomplex by antibody-antigen interaction; secondly, 4-APP was hydrolyzed by ALP and 4-AP subsequently generate, then silver was produced and deposited on Au NBPs surface with the help of 4-AP and accompanied with LSPR peak blue-shifts and color changes.

3.2 Optimization of experimental conditions

In this work, ALP played two important roles, on one hand, it acted as a "bridge", which connected the immune response system with the signal indication unit; on the other hand, as an enzyme hydrolyzed 4-APP to produce 4-AP to participate in the chromogenic reaction. Thus, ALP plays a very important role in this system. According to Gao et al's work, ALP should be better carried out at an effective pH of 9.8 and a working temperature of 37 ℃[41]. Under this condition, some experimental parameters were optimized, including DEA concentration, 4-APP concentration, Ag precursor concentration, and the reaction time. The amount of LSPR peak shifts ($\Delta\lambda_{max}$) were employed as the criterion to evaluate the performance of these conditions. As shown in Figure 2A, the value of $\Delta\lambda_{max}$ increased gradually in case that the concentrations of DEA were below 0.35 M, and reached a platform when the concentrations of DEA were over 0.35 M. Therefore, 0.35 M DEA was chosen as the optimum condition. Similarly, the effect of 4-APP and Ag^+ concentrations were also studied. As shown in Figure 2B and C, $\Delta\lambda_{max}$ increased gradually when the concentration of 4-APP and Ag^+ were below 2 mM and 10 mM, respectively. However, when the 4-APP concentration was larger than 2 mM, $\Delta\lambda_{max}$ would not increase any more. On the contrary, $\Delta\lambda_{max}$ decreased with the further increase of 4-APP concentration. We deduced that the heterogeneous nucleation in case of a relatively high concentration of 4-APP could be the main reason to cause the decrease of $\Delta\lambda_{max}$. It can be seen from Figure 1C that heterogeneous nucleation was obvious when a high concentration of substrate was presented. It is easy to understand that when a high concentration of 4-APP was presented, more Ag^+ would be reduced to Ag simultaneously, while a high concentration of Ag tended to induce heterogeneous nucleation.

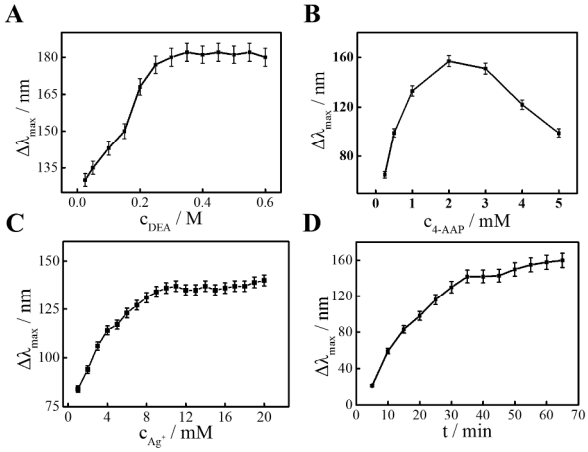

Figure 2 Effect of (A) DEA concentration, (B) 4-APP concentration, (C) Ag^+ concentration and (D) the reaction time on the LSPR peak blue-shift of Au NBPs (All the concentration of ALP used in this was 5.0 mU/mL, n=3).

Finally, the reaction time was investigated. The value of $\Delta\lambda_{max}$ gradually increased when the reaction time was less than 35 min, and reached a platform when the reaction time was between 35 – 45 min. Small increase was observed when the reaction time was over 45 min (Figure 2 D). We inferred that a long reaction time would also induce the formation of heterogeneous nucleation. In this case, most of the silver was coated onto the newly formed silver nanoparticle seeds, while few of them were deposited on Au NBPs@Ag. As shown in Figure S2, the longitudinal LSPR peak almost no shifted and the absorption around 490 nm increasing when the reaction time was

over 45 min. Therefore, 35 min was chosen as the optimal reaction time.

3.3 Detection of ALP

Under the optimum conditions, different concentrations of ALP were incubated with 4-APP, Ag^+ and Au NBPs. The solution exhibits a significant color changes from brownish red to green to dark blue with the increase concentration of ALP (Figure 3A). Continuous blue shift of the extinction peaks were observed when the concentration of ALP was increased from 0.1 to 10 mU/mL. The vivid color changes could be easily distinguished with the naked eye. Thus, semi-quantitative detection of ALP with the naked eye was accomplished. In addition, the UV-vis spectra of the solution containing different concentration of ALP were recorded (Figure 3B). The longitudinal LSPR blue shifted from 755 nm to 595 nm with the ALP concentration increase from 0.1 to 10 mU/mL. The calibration curve exhibited a liner range from 0.1 to 5 mU/mL (Figure 3C), and the detection limit (LOD) for ALP was 0.086 mU/mL ($3\sigma_b$/slope, σ_b represents the standard deviation of blank samples).

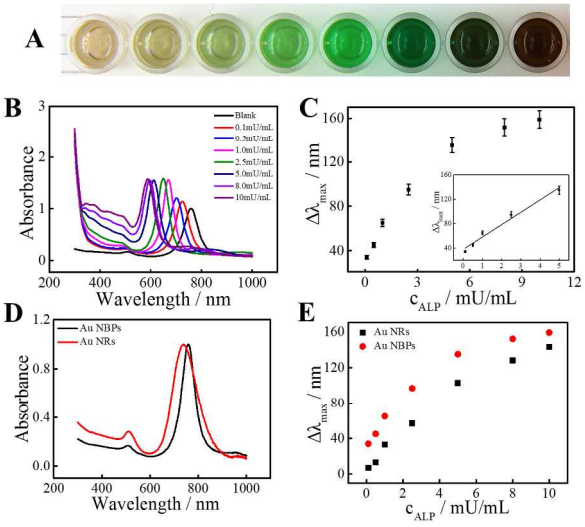

Figure 3 Detection of ALP activity using the proposed colorimetric biosensor. (A) and (B) are photographs and UV-vis spectra in response to different concentrations of ALP; the concentration of ALP in (A) is 0, 0.1, 0.5, 1.0, 2.5, 5.0, 8.0, 10.0 mU/mL (from left to right). (C) is the relationship between longitudinal LSPR blue-shift value ($\Delta\lambda_{max}$) and ALP activity, and the inset in (C) was the calibration curve between $\Delta\lambda_{max}$ and ALP activity. (D) The typical UV-vis spectra of Au NBPs and Au NRs. (E) The comparison of analytical performance of Au NBPs and Au NRs for the detection of ALP activity.

For comparison, we also investigated the different analytical performance between Au NBPs and Au NRs (the UV-vis spectra were shown in Figure 3D). As shown in Figure S3A in the Supporting Information, the color changes between these two nanomaterials were similar. But, it is worth to note that Au NBPs was much more sensitive than Au NRs when detecting low concentration of ALP. As shown in Figure 3E, the Au NBPs LSPR peak blue shifted more than Au NRs at the same concentration of ALP, and that means the color change more obviously and more easily detected by naked eye for the same concentration of ALP.

3.4 Detection of H_5N_1 virus

It is well known that ALP has been widely used as an enzyme label in conventional ELISA. Thus, next we explored the application of the proposed detection strategy for immunoassays. The detection of H_5N_1 virus was selected as a demonstration. As shown in Scheme 1, in our detection scheme, ALP was labelled on the detection antibody by the avidin-biotin system. Thus, the more H_5N_1 viruses existed in the sample solution, the more Ab_2-ALP would adsorb on the ELISA microplate. As a result, the amount of 4-APP hydrolyzed by ALP was in proportional with the concentration of H_5N_1 viruses existed in the sample solution. As shown in Figure 4A and B, with the increase of H_5N_1 virus concentration, the solution color changed from brownish-red to green, dark blue and dark red. Meanwhile, the LSPR peak of the solution blue shifted gradually from 755 nm to 550 nm. When the concentration of the virus protein exceeded 5 ng/mL, no more LSPR peak blue-shift was observed, instead, a little LSPR peak red-shift was appeared. This should mainly come from the evolution of the shape of the nanostructures instead of the optical properties of Ag[39]. Nevertheless, the LSPR blue shifted value $\Delta\lambda_{max}$ has a liner range with virus concentration at the concentration ranging from 1pg/mL to 2.5 ng/mL. The LOD was determined to be 1pg/mL ($3\sigma_b$/slope). Compared with other methods for the detection of influenza virus, the proposed method not only displayed an ultralow LOD but also possessed an additional advantage of semi-quantitative detection of the target with the naked eye (Table S1). Additionally, compared with other noble metal nanomaterials used for colorimetric analysis, the proposed method has a significantly lower LOD and more colorful displays for visual detection (Table S2).

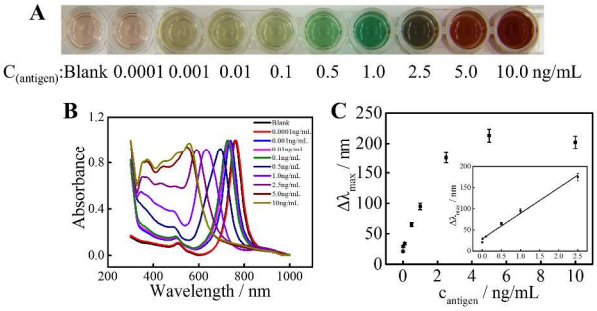

Figure 4 Detection of H_5N_1 virus using the proposed colorimetric immunosensor. Photographs (A) and corresponding UV-vis spectra (B) of the sensor in the presence of different concentrations of H_5N_1 virus antigens. (C) is the relationship between $\Delta\lambda_{max}$ and the antigen concentration.

We further investigated the selectivity of the proposed biosensor. Alpha-fetoprotein (AFP), carcino-embryonic antigen (CEA), human serum albumin (HSA) and H_7N_9 virus were selected as the competitors. As shown in Figure 5, other proteins caused no obvious peak shift and only H_5N_1 induced a

significant LSPR peak shift and corresponding vivid color change. These results indicated that the proposed assay had a good selectivity.

In order to evaluate the potential applicability of the proposed method for clinical diagnostics, mimetic samples containing the normal serum and different concentration of H_5N_1 antigen were tested. As shown in table 1, four mimetic samples were investigated; the results revealed that the proposed assay has a good accuracy and precision with the RSD range of 2.07 ~ 9.41%; and with good recoveries range of 99.00% ~ 102.0%. The corresponding UV-vis spectra of the mimetic samples were shown in Figure S4. Moreover, in order to demonstrate the universality of the proposed sensor, the proposed approach was also demonstrated to detect AFP (Figure S5). Both the solution color and the LSPR spectra are changed significantly with the variations of AFP concentration. These results strongly indicated that our method could be employed for the detection of other biomarkers based on ALP-based ELISA strategy.

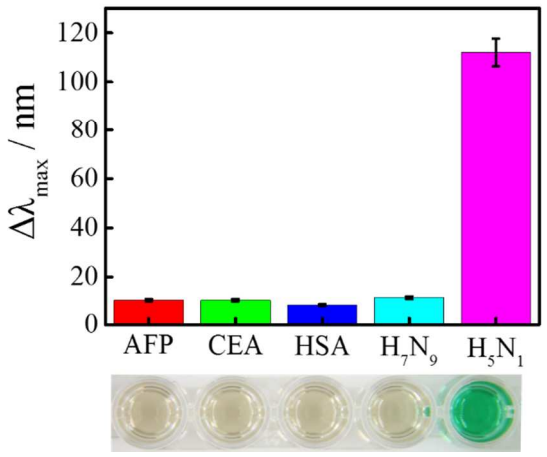

Figure 5 Selective of the proposed assay. The concentration of H_5N_1 was 1.0 ng/mL, and the concentration of all the other proteins were 10 ng/mL.

Table 1 Recoveries and corresponding RSD of the proposed sensor for the detection of H_5N_1 virus antigen added in human serum.

Sample number	1	2	3	4
Added (ng/mL)	0.2	0.5	1	2
Detected (ng/mL)	0.1980	0.4914	1.012	2.039
Recovery rate (%)	99.00	98.28	101.2	102.0
RSD (%)	3.09	2.07	4.14	9.41
Color				

4. Conclusions

In conclusion, we developed an ultrasensitive colorimetric immunoassay method based on target-guided deposition of silver on highly monodispersed Au NBPs. The deposition of silver on Au NBPs generated significant blue shift of the LSPR band. As a result, vivid colors were observed corresponding to different thickness of silver coating. This phenomenon was utilized for the detection of ALP and H_5N_1 virus. The corresponding LODs were 0.086 mU/mL for ALP and 1.0 pg/mL for H_5N_1 virus antigen. Compared with other noble metal nanostructures, colorimetric sensors based on highly monodispersed Au NBPs showed much better sensitivity. In addition, the vivid colors of the proposed sensing strategy enabled us to semi-quantitatively detect the analytes with the naked eye.

ASSOCIATED CONTENT

Supporting Information

The Supporting Information is available free of charge on the ACS Publications website.

AUTHOR INFORMATION

Corresponding Author

Institute of Nanomedicine and Nanobiosensing; Ministry of Education Key Laboratory of Analysis and Detection Technology for Food Safety; College of Chemistry, Fuzhou University, Fuzhou, 350116, China. Tel: 086-591-22866164. Fax: 086-591-22866135. E-mail: guolh@fzu.edu.cn; zylin@fzu.edu.cn.

Notes

The authors declare no competing financial interest

ACKNOWLEDGMENT

This project was financially supported by the Natural Science Foundation of China (21575027, 21675028, 21375021, and 21575025) and the Program for Changjiang Scholars and Innovative Research Team in University (No. IRT1116).

REFERENCES

(1) Kirsch, J.; Siltanen, C.; Zhou, Q.; Revzin, A.; Simonian, A. *Chem. Soc. Rev.* **2013**, *42*, 8733-8768.
(2) Lazcka, O.; Del Campo, F. J.; Munoz, F. X. *Biosens. Bioelectron.* **2007**, *22*, 1205-1217.
(3) Pang, Y.; Rong, Z.; Wang, J.; Xiao, R.; Wang, S. *Biosens. Bioelectron.* **2015**, *66*, 527-532.
(4) Silva, M.; Dias, A. C.; Silva, B. V.; Gomes - Filho, S. L.; Kubota, L. T.; Goulart, M. O.; Dutra, R. F. *J. Chem. Technol. Biotechnol.* **2015**, *90*, 194-200.
(5) Yu, Y.; Chen, Z.; Jian, W.; Sun, D.; Zhang, B.; Li, X.; Yao, M. *Biosens. Bioelectron.* **2015**, *64*, 566-571.
(6) Liu, L.; Wang, X.; Ma, Q.; Lin, Z.; Chen, S.; Li, Y.; Lu, L.; Qu, H.; Su, X. *Anal. Chim. Acta* **2016**, *916*, 92-101.
(7) Paul, A. M.; Fan, Z.; Sinha, S. S.; Shi, Y.; Le, L.; Bai, F.; Ray, P. C. *The Journal of Physical Chemistry C* **2015**, *119*, 23669-23675.
(8) Rakow, N. A.; Suslick, K. S. *Nature* **2000**, *406*, 710-713.
(9) Song, Y.; Wei, W.; Qu, X. *Adv. Mater.* **2011**, *23*, 4215-4236.
(10) Ye, X.; Shi, H.; He, X.; Wang, K.; He, D.; Yan, L. a.; Xu, F.; Lei, Y.; Tang, J.; Yu, Y. *Anal. Chem.* **2015**, *87*, 7141-7147.
(11) Guo, L.; Xu, Y.; Ferhan, A. R.; Chen, G.; Kim, D.-H. *JACS* **2013**, *135*, 12338-12345.
(12) Guo, L.; Ferhan, A. R.; Lee, K.; Kim, D.-H. *Anal. Chem.* **2011**, *83*, 2605-2612.
(13) Jin, R.; Wu, G.; Li, Z.; Mirkin, C. A.; Schatz, G. C. *JACS* **2003**, *125*, 1643-1654.

(14) Yu, C.; Irudayaraj, J. *Anal. Chem.* **2007**, *79*, 572-579.
(15) Mayer, K. M.; Lee, S.; Liao, H.; Rostro, B. C.; Fuentes, A.; Scully, P. T.; Nehl, C. L.; Hafner, J. H. *Acs Nano* **2008**, *2*, 687-692.
(16) Ma, X.; Chen, Z.; Kannan, P.; Lin, Z.; Qiu, B.; Guo, L. *Anal. Chem.* **2016**, *88*, 3227-3234.
(17) Wang, D.; Guo, L.; Huang, R.; Qiu, B.; Lin, Z.; Chen, G. *Electrochim. Acta* **2014**, *150*, 123-128.
(18) Chen, H.; Shao, L.; Li, Q.; Wang, J. *Chem. Soc. Rev.* **2013**, *42*, 2679-2724.
(19) Vigderman, L.; Khanal, B. P.; Zubarev, E. R. *Adv. Mater.* **2012**, *24*, 4811-4841.
(20) Li, Q.; Zhuo, X.; Li, S.; Ruan, Q.; Xu, Q. H.; Wang, J. *Advanced Optical Materials* **2015**, *3*, 801-812.
(21) Liu, M.; Guyot-Sionnest, P.; Lee, T.-W.; Gray, S. K. *Physical Review B* **2007**, *76*, 235428.
(22) Kou, X.; Ni, W.; Tsung, C. K.; Chan, K.; Lin, H. Q.; Stucky, G. D.; Wang, J. *Small* **2007**, *3*, 2103-2113.
(23) Chen, H.; Kou, X.; Yang, Z.; Ni, W.; Wang, J. *Langmuir* **2008**, *24*, 5233-5237.
(24) Lee, S.; Mayer, K. M.; Hafner, J. H. *Anal. Chem.* **2009**, *81*, 4450-4455.
(25) Guo, Z. R.; Wan, Y.; Wang, M.; Xu, L.; Lu, X.; Yang, G.; Fang, K.; Gu, N. *Colloids and Surfaces a-Physicochemical and Engineering Aspects* **2012**, *414*, 492-497.
(26) Zhang, H.; Liu, J. *Opt. Lett.* **2016**, *41*, 1150-1152.
(27) Liu, W. J.; Liu, D.; Zhu, Z. N.; Han, B.; Gao, Y.; Tang, Z. Y. *Nanoscale* **2014**, *6*, 4498-4502.
(28) Li, Q.; Zhuo, X.; Li, S.; Ruan, Q.; Xu, Q.-H.; Wang, J. *Advanced Optical Materials* **2015**, *3*, 801-812.
(29) Signorini, M.; Lottersberger, J.; Tarabla, H.; Vanasco, N. *Epidemiology and infection* **2013**, *141*, 22-32.
(30) Lang, Q.; Wang, F.; Yin, L.; Liu, M.; Petrenko, V. A.; Liu, A. *Anal. Chem.* **2014**, *86*, 2767-2774.
(31) Bu, D.; Zhuang, H.; Zhou, X.; Yang, G. *Talanta* **2014**, *120*, 40-46.
(32) Cui, Y.; Liu, K.; Xu, C.; Liu, F.; Li, Q. X.; Liu, S.; Wang, B. *Food Chem.* **2014**, *143*, 293-299.
(33) Zhang, M.; Yu, X.; Wang, Y.; Hu, Y.; Liu, S. *Food Analytical Methods* **2013**, *6*, 1223-1228.
(34) Lu, Y.; Peterson, J. R.; Gooding, J. J.; Lee, N. A. *Analytical and bioanalytical chemistry* **2012**, *403*, 1607-1618.
(35) de la Rica, R.; Stevens, M. M. *Nat Nanotechnol* **2012**, *7*, 821-824.
(36) Zhang, H.; Ma, X.; Hu, S.; Lin, Y.; Guo, L.; Qiu, B.; Lin, Z.; Chen, G. *Biosens. Bioelectron.* **2016**.
(37) Tang, L.; Li, S.; Xu, L.; Ma, W.; Kuang, H.; Wang, L.; Xu, C. *ACS Appl Mater Interfaces* **2015**, *7*, 12708-12712.
(38) Xiang, Y.; Wu, X.; Liu, D.; Li, Z.; Chu, W.; Feng, L.; Zhang, K.; Zhou, W.; Xie, S. *Langmuir* **2008**, *24*, 3465-3470.
(39) Zhu, X.; Zhuo, X.; Li, Q.; Yang, Z.; Wang, J. *Adv. Funct. Mater.* **2015**, *26*, 341-352.
(40) Xiang, Y.; Wu, X.; Liu, D.; Li, Z.; Chu, W.; Feng, L.; Zhang, K.; Zhou, W.; Xie, S. *Langmuir* **2008**, *24*, 3465-3470.
(41) Gao, Z.; Deng, K.; Wang, X.-D.; Miró, M.; Tang, D. *ACS applied materials & interfaces* **2014**, *6*, 18243-18250.

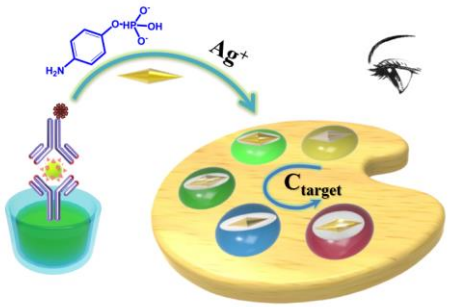

For TOC only